Fatih ALTINDİŞ USAGE OF LASER INDUCED BUBBLES FOR MEASURING INTRAOCULAR EYE PRESSURE AGU 2017

USAGE OF LASER INDUCED BUBBLES FOR MEASURING INTRAOCULAR EYE PRESSURE

A THESIS
SUBMITTED TO THE DEPARTMENT OF ELECTRICAL AND COMPUTER ENGINEERING
AND THE GRADUATE SCHOOL OF ENGINEERING AND SCIENCE OF ABDULLAH GUL UNIVERSITY
IN PARTIAL FULFILLMENT OF THE REQUIREMENTS
FOR THE DEGREE OF
MASTER IN SCIENCE

By
Fatih ALTINDİŞ
December 2017

USAGE OF LASER INDUCED BUBBLES FOR MEASURING INTRAOCULAR EYE PRESSURE

A THESIS
SUBMITTED TO THE DEPARTMENT OF ELECTRICAL AND COMPUTER ENGINEERING
AND THE GRADUATE SCHOOL OF ENGINEERING AND SCIENCE OF ABDULLAH GUL UNIVERSITY
IN PARTIAL FULFILLMENT OF THE REQUIREMENTS
FOR THE DEGREE OF
MASTER IN SCIENCE

By
Fatih ALTINDİŞ
December 2017

SCIENTIFIC ETHICS COMPLIANCE

I hereby declare that all information in this document has been obtained in accordance with academic rules and ethical conduct. I also declare that, as required by these rules and conduct, I have fully cited and referenced all materials and results that are not original to this work.

Fatih ALTINDIŞ

REGULATORY COMPLIANCE

M.Sc. thesis titled USAGE OF LASER INDUCED BUBBLES FOR MEASURING INTRAOCULAR PRESSURE has been prepared in accordance with the Thesis Writing Guidelines of the Abdullah Gül University, Graduate School of Engineering & Science.

Prepared By	Advisor
Fatih ALTINDIŞ	Prof. Bülent YILMAZ

Head of the Electrical and Computer Engineering Program
Assoc. Prof. V. Çağrı GÜNGÖR

ACCEPTANCE AND APPROVAL

M.Sc. thesis titled USAGE OF LASER INDUCED BUBBLES FOR MEASURING INTRAOCULAR PRESSURE and prepared by Fatih Altındiş has been accepted by the jury in the Electrical and Computer Engineering Graduate Program at Abdullah Gül University, Graduate School of Engineering & Science.

…….. /…….. / ……..

JURY:

Advisor	: Prof. Bülent YILMAZ
Member	: Assoc. Prof. İbrahim Tuna ÖZDÜR
Member	: Assoc. Prof. Ayşegül GÜVEN

APPROVAL:

The acceptance of this M.Sc. thesis has been approved by the decision of the Abdullah Gül University, Graduate School of Engineering & Science, Executive Board dated ….. /….. / …….. and numbered ……..……. .

…….. /…….. / ……..

(Date)

Graduate School Dean
Prof. İrfan Alan

ABSTRACT

USAGE OF LASER INDUCED BUBBLES FOR MEASURING INTRAOCULAR PRESSURE

Fatih ALTINDİŞ
MSc. in Electrical and Computer Engineering
Supervisor: Prof. Bülent YILMAZ

December 2017

There are different methods of measuring intraocular pressure in clinics, but those methods fail to measure intraocular pressure under certain conditions. Most common problem of these methods are that they are inapplicable to patients who had eye surgery. In this study laser induced bubble characteristics are investigated in order to develop a new method to measure intraocular eye pressure with lasers. For this purpose, first, intraocular environment is imitated to perform laser experiments. Then imaging system is developed to digitally visualize laser induced bubbles that are created in intraocular-like environment. Digital image processing algorithms were developed to detect and measure bubble features. Different fluid pressure levels were configured to investigate the pressure effect on laser induced bubbles. Results showed that volume of laser induced bubbles are higher in lower fluid pressure and bubble volume decrease with the increased fluid pressure. In light of these findings, it can be concluded that the change in volume can be used to estimate fluid pressure. Thus, this study proposes a new technique for measuring intraocular pressure by using volume feature of laser induced bubbles that are created in the anterior chamber of the eye.

Keywords: Laser induced bubbles, Cavitation bubbles, Intraocular pressure, Digital image processing, Glaucoma

ÖZET

LAZER İLE OLUŞTURULAN KABARCIKLARIN GÖZİÇİ BASINÇ ÖLÇÜMÜNDE KULLANIMI

Fatih ALTINDİŞ
Elektrik ve Bilgisayar Mühendisliği Bölümü Yüksek Lisans
Tez Yöneticisi: Prof. Dr. Bülent YILMAZ
Aralık 2017

Günümüzde göz tansiyonu ölçmeye yönelik farklı yaklaşımlar kullanılmaktadır. Ancak, bu yaklaşımlar bazı durumlarda hastaların göz tansiyonunu ölçmekte zorlanmaktadır. En fazla sıkıntı yaşanan durum, gözünden ameliyat geçirmiş kişilerin göz tansiyonunu ölçme konusunda yaşanmaktadır. Bu kişilerin korneası ameliyat sonrası hassaslaştığı için tonometre cihazları ile göz tansiyonu ölçülememektedir. Bu tez çalışması, 1064 nm dalga boyunda çalışan bir Nd:YAG lazer ile sıvı içerisinde oluşturulan kabarcıkların karakteristiğini inceleyerek, göz tansiyonunu bu kabarcıkların boyutlarından ölçmeye yönelik yeni bir yaklaşım geliştirmeyi amaçlamıştır. Bu doğrultuda, öncelikle göz içi ortamına benzeyen yapay bir ortam tasarlanmıştır. Bu ortam içerisinde lazer ile oluşturulan kabarcıkları takip edecek bir görüntüleme sistemi ve bu sisteme entegre çalışan bir görüntü işleme yazılımı geliştirilmiştir. Farklı sıvı basınçlarında lazer ile oluşturulan kabarcık görüntüleri işlenerek kabarcıklara ait özellikler çıkarılmıştır. Sonuçlar göstermiştir ki, lazer ile oluşturulan kabarcıkların hacimleri düşük basınç altında daha fazla olurken, sıvı basıncı arttıkça bu kabarcıkların hacmi azalmaktadır. Elde edilen veriler ışığında, kabarcıklarda meydana gelen bu hacim değişiminin, kabarcığın içinde bulunduğu sıvının basıncını ölçmekte kullanılabileceği sonucuna varılmıştır. Bu çalışma, lazer ile sıvı içerisinde oluşturulan kabarcıklar ile ilgili elde edilen bu verileri kullanarak, gözün ön kamarasında lazer ile kabarcık oluşturmaya ve göz içi basıncını bu kabarcık yardımıyla ölçmeye yönelik yeni bir yaklaşım geliştirmeyi önermektedir.

Anahtar kelimeler: Lazer ile oluşturulan kabarcık, Kavitasyon baloncukları, Göz içi basıncı, Dijital görüntü işleme, Glokom

Acknowledgements

This study is supported by TÜBİTAK 1512 Entrepreneur Gradual Support Program.

Table of Contents

List of Figures

Chapter 1

Introduction

The introduction of short pulse lasers has breakthrough effects on treatments for eye related inconveniences, because it enables non-invasive surgical operations on eyes. LASIK (Laser assisted in situ keratomileusis) surgeries are used to correct optical defects such as myopia, hyperopia and astigmatism [1]. Nd:YAG laser treatments are used for cataract by cleaning out clouding in lenses. However developed laser technology brings out new drawbacks for patients who have laser surgery for ocular disorders. After the laser surgery, patients corneas become very fragile for any outside force because of the exposed energy on tissues [2], [3]. Thus, some routine measurement controls such as intraocular pressure (IOP) control have become inapplicable to these patients.

While short pulse laser technology is used in many areas of ocular operations [3], [4], it is not used in IOP measurement devices (ocular tonometry) to solve usage difficulties of traditional tonometers that encountered in some clinical cases. The reason behind difficulties is that ocular tonometers still use invasive methods in order to measure IOP value. Ocular tonometers can measure IOP values by whether applying direct physical force to cornea or applying air pressure to cornea. However, both of these methods are extremely discomfortable for patients and it is not even suggested to use those tonometers on patients who had laser surgery [5]–[7].

Another usage of short pulse lasers is to create bubbles in fluids by heating and vaporizing small portion of fluid. If the lasers are aimed inside of the fluid, vaporized fluid particles create bubble and it starts to rise up [8]–[15]. However, none of these studies focused on relationship between fluid pressure and laser induced bubbles.

In this thesis study, first, laser induced bubbles are examined in different fluids in order to understand the effect of viscosity on bubbles' behavior. Then, the effect of different fluid pressure levels on laser induced bubbles are examined. These two experiment concepts can be linked together in order to measure IOP of human eye and non-invasive IOP measurement technique can be developed. For this purpose, first laser induced bubbles should be created in intraocular fluid and then bubbles are followed by a digital camera. Bubbles' behavior inside of intraocular fluid is analyzed by digital image processing tools. The results showed that there is a difference in bubble behavior for different pressure levels and it can be used to find a link between fluid pressure and bubble behavior.

This study showed detailed investigation of bubbles' behavior in different intraocular-like environments and proposed that IOP values can be measured by a compact system which includes short pulse laser, digital microscopic imaging system and image processing software.

Next chapter will explain detailed background information about eye anatomy, IOP and laser induced bubbles. Third chapter will investigate emergence of laser induced bubbles and their motion inside of the fluids. Digital image processing techniques that are used to track down and evaluate bubbles' behaviors, are also discussed in that chapter. Results and further suggestions are discussed in the fourth chapter.

Chapter 2

Structure of Eye and Laser

2.1 Eye Anatomy

Eyes are the vital part of human visual ability. They reach their final shape in mother's womb and keep that shape and structure until individual's death. Therefore, ocular tissues have an unrenewable form that is highly sensitive and fragile to any outside force. Eye has a spherical shape and three surrounding tissue layers around. Outmost tissue layer called sclera. Sclera has white, hard and fibrous structure and gives hardness and durability to eye. Middle layer tissue, called choroid, contains connective tissues between sclera and retina. Choroid provides oxygen and nourishment to outer cells of retina. Innermost and the third layer tissue is called retina. Retina contains light sensitive cells and convert lights into bio-electrical signals.

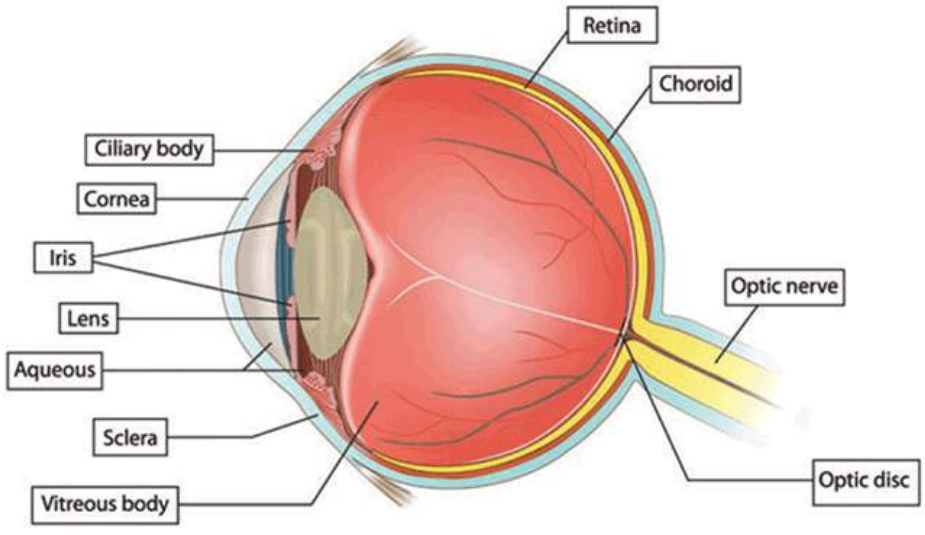

Figure 2.1.1 Anatomy of eye is visualized.

There is a transparent area in the front of the eye where sclera ends. This transparent area is called cornea which contains transparent cells. Cornea lets light inside of the eye, and also provides elasticity to the eye. Iris is located behind the cornea and adjusts amount of light that passes through by changing pupil's radius. Lens is placed behind the iris. It refracts light beams and focuses them on the retina. The volume inside of the eye is filled with a transparent fluid called the vitreous. This fluid contains oxygen and nourishment for lens and inner cells of the retina. Also, vitreous support spherical shape of the eye. The blank area between cornea and iris is called the "anterior chamber" which is also filled with fluid. Figure 2.1.1 shows and summarizes general anatomy of the human eye [16].

2.1.1 Anterior Chamber

The volume between cornea and iris is called the anterior chamber. Backside of the anterior chamber has iris and the ciliary body. Ciliary body is composed of small muscles that enables iris to get enlarge or tighten. It also excretes humor aqueous fluid which nourishes cornea cells. The fluid excreted from ciliary body circulates through pupil and exits from small openings between where cornea and iris meet. These small openings are called trabecular meshwork and Schlemm's canal. Figure 2.1.1.1 shows a closer look to anterior chamber and trabecular meshwork.

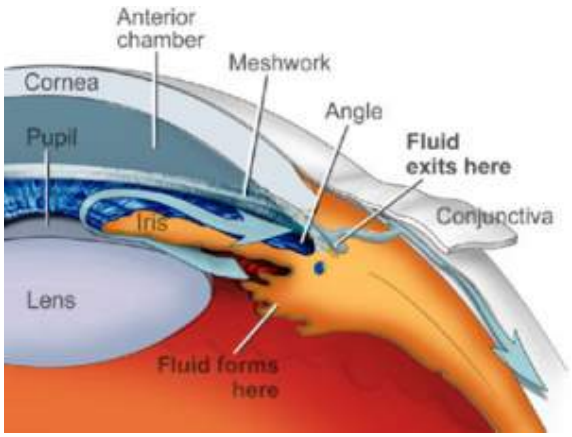

Figure 2.1.1.1 A closer look to anterior chamber explains circulation of humor aqueous. It is excreted from ciliary body, flows through pupil and exits from trabecular meshwork.

Humor aqueous and vitreous fluids fill inside of the eye and creates inner pressure. This pressure tries to push-out sclera. Also, sclera tries to squeeze eye because of its hard and tight structure. These bidirectional forces create pressure inside of the eye that gives spherical shape to the eye and keeps it healthy. Intraocular pressure supports circulation of humor aqueous and vitreous fluids. For this circulation, trabecular meshwork and Schlemm's canal has vital role, because excreted fluids can only exit through these openings. Thus, trabecular meshwork and Schlemm's canal are the control mechanisms for intraocular pressure. If they evacuate too much fluids, intraocular pressure decreases suddenly. On the contrary, if those openings do not evacuate enough fluids, intraocular pressure increases. Both of the cases are highly dangerous for eye health.

2.1.2 What is Glaucoma?

Glaucoma is the name for group of eye diseases that damage optic nerves and retina which eventually results in blindness. Glaucoma almost has no symptoms in early stages and when it is diagnosed, it is often too late to recover patient's vision loss. Glaucoma is often caused by increased intraocular pressure.

Intraocular pressure is created by humor aqueous fluid that is excreted from ciliary body, and trabecular meshwork evacuate this fluid in order to keep intraocular pressure level in balance. However, if trabecular meshwork cannot evacuate enough fluid, then humor aqueous fluid pressure to sclera starts to increase. It can be imagined as blowing a balloon. If there is too much air blown into the balloon, it pops. Thankfully, sclera is very strong and increased intraocular pressure does not result eye popping, but it starts to suppress most fragile tissues of sclera of the eye, which is the optic nerve. This pressure causes a damage on optic nerves starting from inner layers to outer layers. There are two main glaucoma types; open-angle glaucoma and closed-angle glaucoma.

Open-angle glaucoma is the type where IOP slowly increases and damages optic nerve, which results in the loss of vision. It can develop in years without any symptoms. On the other hand, closed-angle glaucoma is acute attacks of high pressure which causes nausea, eye pain and blurred vision. Also, there is a less

common type glaucoma called normal-tension glaucoma which shows normal signs of intraocular pressure but damages the optic nerve and causes blindness.
Risk factors of glaucoma are age, family history of the condition, high blood pressure and obesity. Also, darker working environments increase intraocular pressure in short time periods [17]–[19]. However, glaucoma can be treated if it is diagnosed on time. Glaucoma treatments basically tries to increase fluid circulation or decrease amount of excreted fluid.

2.1.3 Intraocular Pressure Measurement

Importance of intraocular pressure and risks of high intraocular pressure were discussed in previous sections. This section focuses on the measurement techniques of intraocular pressure (IOP). IOP measurement devices are called as ocular tonometer and there are basically two types of tonometer devices that are available on the market. Both of them needs physical interference from outside of the cornea to measure IOP of the patients.
First one directly applies a physical force to patient's cornea and measure resistance force coming back from the eye itself. This method gives very accurate results, however it is very uncomfortable even for patients who haven't had any laser treatment, since the human instinct of preventing eyes from any outside interference is so hard to suppress. Also, it is inapplicable to patients who had a laser surgery because their corneas become very sensitive after the laser treatment. Another reason of inapplicability of this tonometer is that patient's cornea loses its natural anatomical structure after the laser surgery, and this causes false measurements about intraocular pressure even years after the surgery. Figure 2.1.3.1 shows how this tonometry works.

Figure 2.1.2.1 Applanation tonometer is directly applied to the cornea to measure intraocular pressure.

The second tonometry device is called as air tonometry or air puff tonometry. This tonometry measures IOP by puffing air to patient's cornea and tracks the corneal resilience. Figure 2.1.3.2 shows air tonometer.

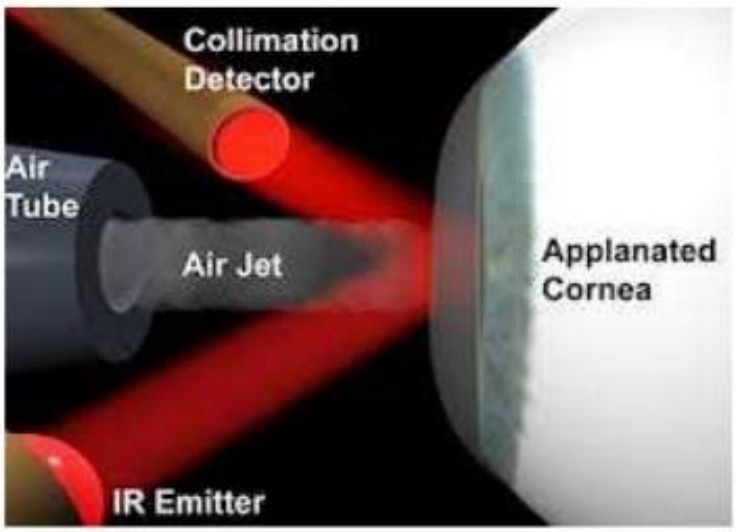

Figure 2.1.3.2 Air puff tonometer puffs air onto the cornea and tracks down its resilience to measure intraocular pressure.

This method can mislead doctors occasionally and needs a correction table in order to give accurate results. Cornea resilience depends on a couple of parameters besides IOP. Cornea thickness effects resilience of cornea and if cornea is thicker than referred thickness value, air tonometer will measure higher IOP value than actual IOP value. If cornea is thinner than referred thickness value, air tonometer will yield a lower IOP value than the actual IOP value. In order to correct those measurements, doctors need a correction table and also, they need to know patient's cornea thickness. Pachymeters are devices that measure cornea thickness. Then, ophthalmologists refer to the correction table and calculate the actual IOP value with measurements coming from the air tonometer and the pachymeter. This is a very long and non-practical way to measure the exact IOP value. Moreover, air tonometers are also inapplicable to patients who had laser surgery, because, this method also applies physical force to the cornea for IOP measurement. This situation results in impractical conditions for doctors when it comes to clinical applications for IOP measurement.

Both of the methods are very prevalent for IOP measurements especially air tonometer, even they have disadvantages, because those tonometers provide cheaper and faster results to the doctors. However, after a laser surgery such as LASIK or filtering microsurgery, doctors need to track patient's IOP values. But available devices cannot be used accurately on these patients since their corneas have become very fragile and sensitive after the surgery.

2.2 Laser Induced Bubbles

Laser induced bubbles mean bubbles that are generated by the focused laser beams inside of a fluid by vaporizing the fluid. There are many different names for laser induced bubbles such as vapor bubbles, laser induced cavitation bubbles [8]–[11]. In this study, "*laser induced bubble*" term is used to refer to those bubbles.

Before examining detailed structure and characteristic of laser induced bubbles, it is useful to understand how short pulse lasers work. Short pulse lasers work with one laser module. The term *short pulse* refers to very strong laser beams that is only performed in nanoseconds [20]–[22]. Generated laser beam is splitted with a beam splitter, and then two beams are aimed to intersect at a certain point. At the intersection point of splitted laser beams, great level of energy is emerged because of high energy that beams carry. If laser beams aimed to intersect in air, they can create a spark. If the laser beams aimed to intersect in a fluid, then the intersection point heats up suddenly and vaporize small portion of fluid and generate a bubble. There are different types of elements that are used to create laser beams, in this study Nd:YAG type lasers are used to create laser induced bubbles.

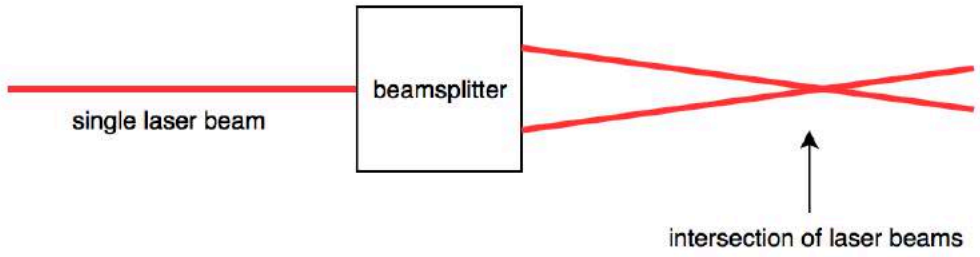

Figure 2.2.1 Laser beam is splitted and then intersected at a point where great level of energy is obtained.

2.2.1 Creation of Bubble

Laser induced bubbles are generated by aiming and intersecting laser beams inside of a fluid. Laser beams heat up the fluid in a very short period of time. After some point heat of the fluid passes the breakdown temperature and heated fluid forms the plasma [23], [24]. If the heating up continues plasma becomes vapor and forms a bubble. First formed bubble starts to enlarge and as it gets larger gas pressure

inside the bubble decreases. At some point, bubble loses its impulse energy that is created by laser and also gas pressure inside of the bubble drops, which stops enlargement of bubble walls, and shrinking begins. Bubble shrinks down and collapse, then this sudden collapse creates jet flow and shock wave [11], [20], [21], [23]–[31]. Figure 2.2.1.1 is taken from [10] and it shows first collapse of bubble and jet flow.

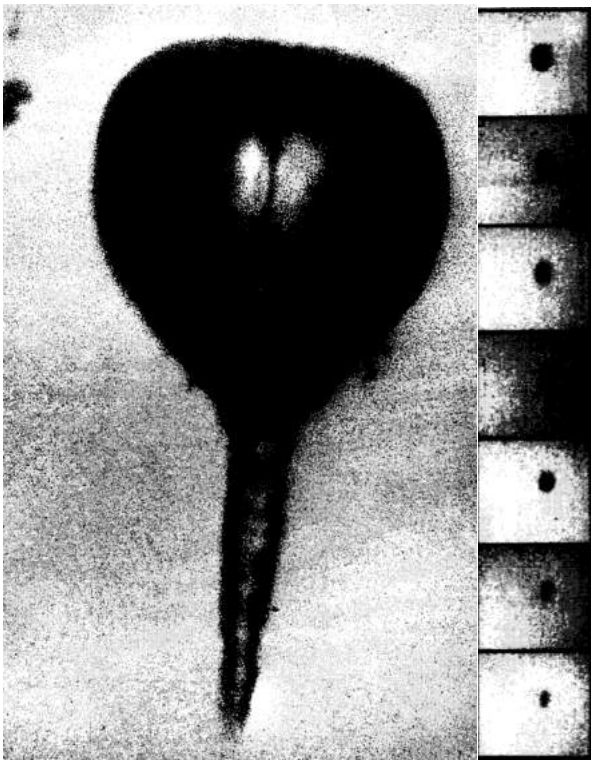

Figure 2.2.1.1 Jet flow is showed on left. It forms with the collapse of the bubble. Bubble collapse is showed in serial images on the right side of the image.

After the collapse, bubble starts to enlarge again. This enlargement - shrinking circle continues couple of times and finally bubble reaches steady state and stops enlarging or shrinking significantly. After this point bubble starts rising up with a linear speed because of fluids buoyancy. While bubble is rising, vapor gets cooler and condense and diffuse into fluid, which causes bubbles volume to dwindle.

2.2.2 Shockwaves

Shockwaves are emitted during the collapse of bubble and they contain high

amount of energy and pressure [20], [25], [30], [32]. This energy has a corrosive effect on solid materials. There are many studies that shows the effect of shockwaves on solid materials [33]–[36]. In addition, shockwaves are used in cataract surgeries to clean out clouding on lenses. Shockwaves create high pressure in fluid when they emerged and this pressure corrode material that shockwaves hit. Figure 2.2.2.1 shows serial photographs of bubble collapse and shockwave emissions [10].

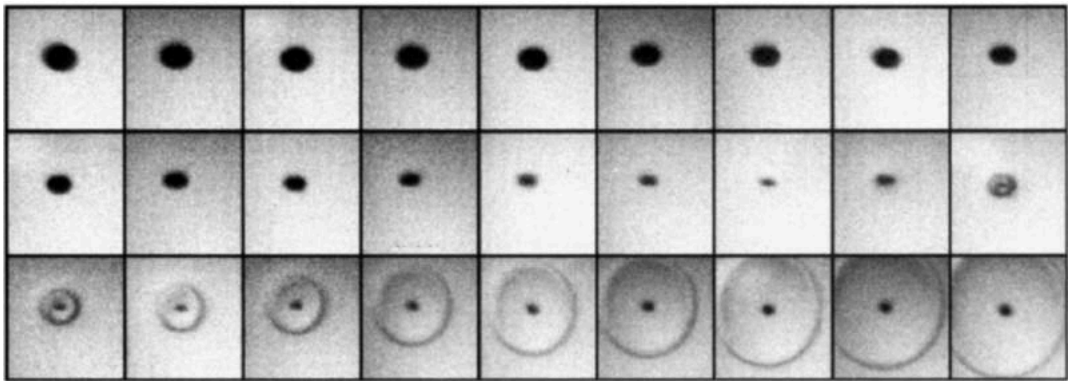

Figure 2.2.2.1 Shockwaves are showed in third row. They propagate after bubble collapsed, which is showed in first and second row.

It can be seen that shockwaves emerge with the collapse of laser induced bubble. Shockwaves propagate faster than bubble walls, because they have more energy. When shockwaves hit to a surface, reflected waves provide information about resilience of that surface. While solids absorb energy of shockwaves and reflect only small portion of it, elastic surfaces reflect shockwaves better and they absorb less energy from the shockwaves. Thus, shockwaves cause more corrosion on solid surfaces than elastic surfaces.

Chapter 3

Materials and Methods

In this thesis study, it is proposed that laser induced bubbles can be generated in the anterior chamber of the eye, and they can be tracked with a digital camera system in order to measure intraocular pressure of the eye. It is important to choose the location of a bubble to be generated away from the critical tissues in the eye because emitted shockwaves can damage those tissues [2], [3], [37]. The best possible location for creating laser induced bubbles in the eye is the anterior chamber. Anterior chamber is chosen for laser shots because it has very large space between center of the cornea and iris. Thus, effects of shockwaves of laser induced bubbles on cornea and iris tissues are expected to be minimized and can be repairable.

Another aspect of choosing anterior chamber is that it provides essential conditions for visualization techniques. Anterior chamber is covered with cornea on the outer side. Since cornea has a transparent curved structure, it is easy to visualize anterior chamber through cornea from different angles.

3.1 Required Tools and Materials

In order to generate laser induced bubble inside of anterior chamber and measure the bubble size, hardware and software tools are used in this study.

3.1.1 Laser

Short pulse laser devices can create bubbles inside a fluid as it is discussed in the previous chapter. In clinical approaches, one of the most preferred short pulse

laser type is Nd:YAG (neodymium doped-ytrium aluminium garnet) laser. Nd:YAG type laser which is used in hospital clinics, is also used in this study. This system is shown in figure 3.1.1.1.

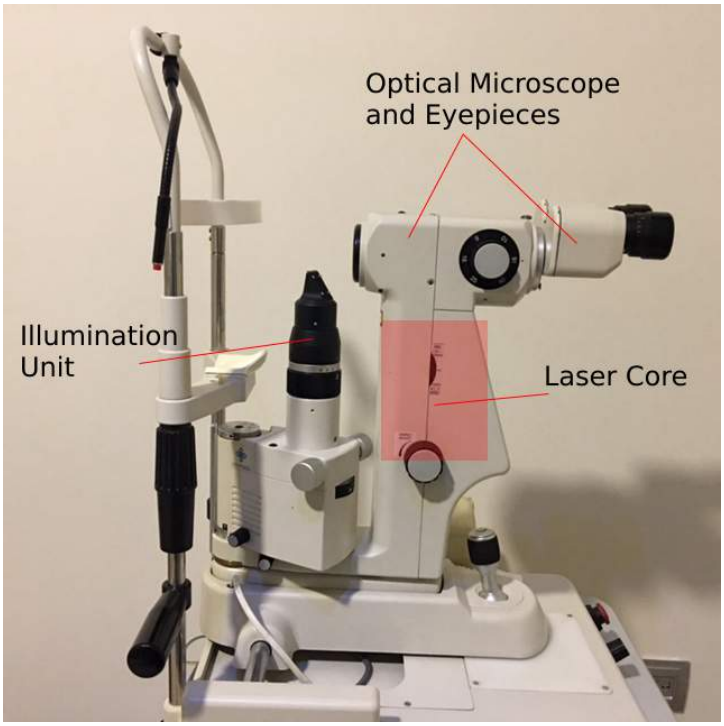

Figure 3.1.1.1 Nd:YAG compact laser system is composed of laser, optic microscope and illumination unit.

Clinical laser devices are compact designs that include Nd:YAG laser, guide light, slit illumination unit and optical microscope. Particular laser that is used in this study, is *lightmed* brand and its application fields are mostly for capsulotomy and membranectomy. Its laser has 1064 nm wavelength with 4 nanoseconds pulse-width. It has energy range between 0.2 mJ and 10 mJ. Its microscope has magnification options from 5X to 40X. Also, laser can be fired with up to 45-degree angle from the center to the left or right. There is an illumination unit on the device which provides slit light to laser focus in order to brighten laser application area. These specifications are very feasible for the concept of our study.

3.1.2 Integration Part for Imaging System

In order to visualize exact spot where lasers are aimed and laser induced bubbles are formed, imaging system should be aligned with the optic center of the laser system. For this purpose, laser system is investigated and two possible solution ideas have evolved.

First solution offers to use laser systems included optic microscope for imaging bubbles. This can be accomplished by adding a beam splitter in front of one of the microscope eyepieces. Then imaging system can be added on the third eyepiece and common visual output would be achieved. However, laser system producers do not allow any changes after they completed the design of ordered product. Since in this study we used the laser system of an eye clinic, it was not possible to change laser system design for the time that study was conducted.

Figure 3.1.2.1 Beam splitters can be attached in front of the eyepieces and provide one extra mount for attaching digital camera to the laser system.

Second solution offers a different approach that requires no need to alter the laser system design. In this approach, it is proposed to attach an arc shaped metallic

piece to illumination kit of laser system as it shown in figure 3.1.2.2.

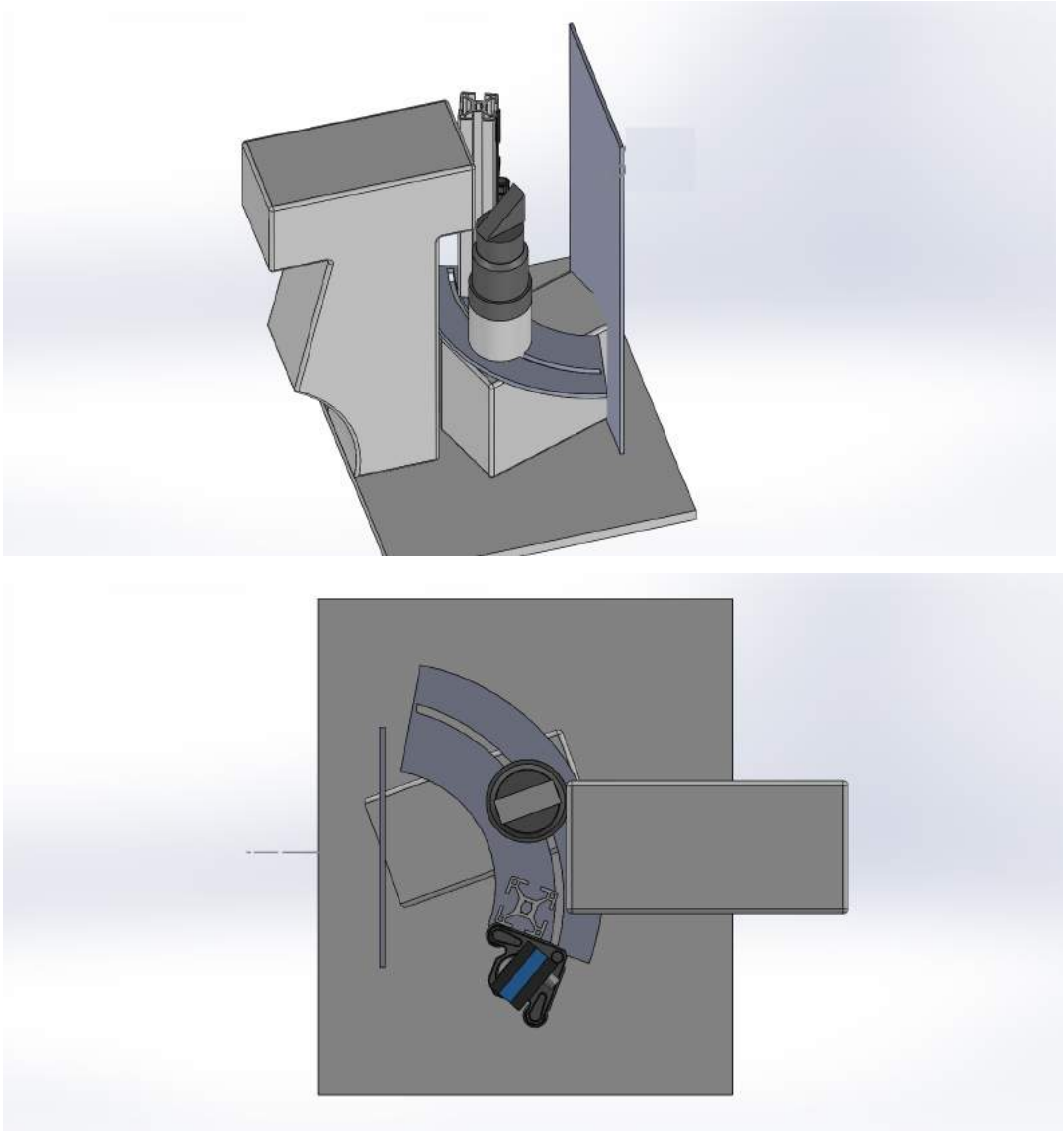

Figure 3.1.2.2 Arc attachment is planned and modelled. Model of plan how arc is attached to the laser system is shown from different angles.

This arc shaped metallic piece has its center at the same spot where laser system has. Then imaging system attached on this arc and it provided visualization of the same spot from different angles. This approach does not require changing the laser system design, instead it adapts to the available design thanks to this arc shape.

Figure 3.1.2.3 Arc is created with a CNC system.

Figure 3.1.2.3 shows metallic arc and the figure 3.1.2.4 shows how it is integrated to the laser system. However, this solution could not be used, because during the study, imaging system camera was switched to a different type of camera system. The new system was not compatible with this solution. Imaging systems and final approach of integration part is discussed in section 3.1.3.

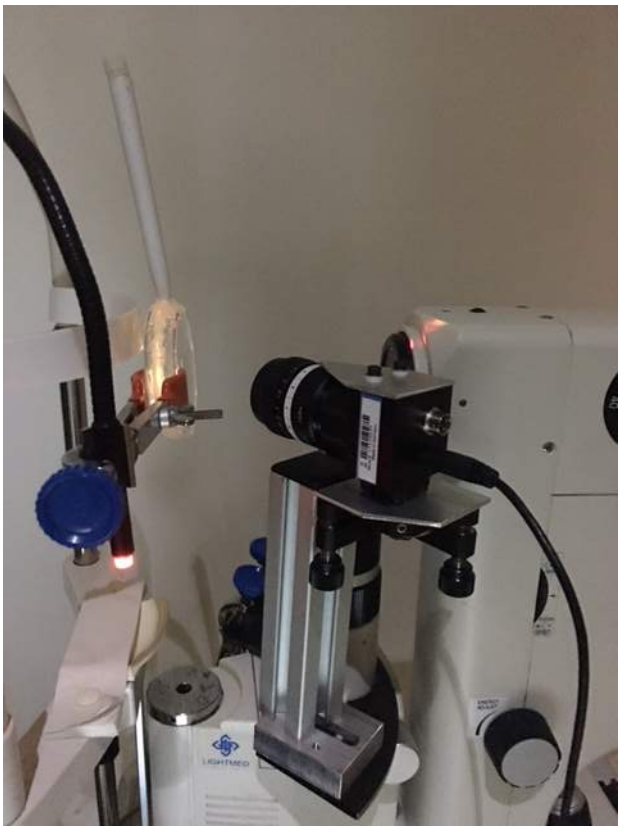

Figure 3.1.2.4 A photo of how imaging system works after arc was attached to the laser system.

3.1.3 Imaging System

Imaging system was a very important element for this study, because further operations of this study relied on images of laser induced bubbles. Therefore, imaging system should be stable, fast and reliable. Three different imaging systems had been tested in this study in order to capture the best images of laser induced bubbles.

First system was composed of three kits; metallic footing for the camera, fine level adjustment kit and the digital camera. Digital camera has a CCD image sensor, with rolling shutter, 30 frames per second filming rate and 1280 x 1024 pixel resolution, also it has configurable zoom up to 5X. Figure 3.1.3.1 shows digital camera and its configurable parts.

Figure 3.1.3.1 CCD camera and its metallic footing is shown from two different angles.

Second integration solution in section 3.1.2 was specifically designed for this imaging system. This system also had an available free software for analyzing images that are taken with this camera system. It has built-in particle analyzer

which could be useful to detect and measure bubbles.

Second system was a compact digital microscope system, which was widely used in many studies especially analysis of circuit boards, because this camera can zoom up to 500x (50x optic, 10x digital zoom) and it has 30 frames per second filming rate. Figure 3.1.3.2 shows physical appearance of this camera. These technical features of the camera can provide enough magnification for visualizing laser induced bubbles.

Figure 3.1.3.2 Digital microscope camera and its data transfer cable

For the third and final imaging system, smartphone cameras have chosen, because they can provide higher frame rate and higher resolution to capture bubbles. Chosen smartphone model was iPhone 7, because it can record video with 240 frames per second filming rate in slo-mo option and provides 720p resolution.

Detailed advantages and disadvantages of each imaging system is discussed in section 3.2.

3.1.4 Intraocular-like Environment

Another important parameter was to determine the fluid environment that can imitate intraocular environment. Since the final goal was the measure intraocular pressure, it was important to create fluid environment that is close to humor aqueous. Also, it was important to have the option to change pressure of the fluid systematically. For this purpose, leak-proof glass cuvettes were chosen as a fluid container, because they are made of thin transparent glasses that do not alter laser power.

Figure 3.1.4.1 Leak-proof glass cuvette.

Fluids that were chosen for experiments had two common features which are purity and accessibility. Purity is important to repeat identical laser induced bubbles, because contaminated fluids include different floating particles inside which may affect generation of laser induced bubbles. Moreover, it is not possible to measure contamination level of the fluid which disables calculating the fluid density correctly. Also, accessibility of fluid is important for repeating

experiments in different times and places. That is why, pure water and baby oil were used in these experiments. Both are easy to access and are sterilized from foreign particles. While pure water provides closer intraocular environment in terms of fluid density, laser induced bubbles in pure water rise very fast because of water buoyancy. On the other hand, even though baby oil has lower density from humor aqueous, bubbles rise slower in baby oil which provides a better opportunity to capture bubble images.

3.1.5 Image Processing Software

Creating repeatable laser induced bubbles and capturing the bubble images correctly were important steps for this study, but processing those images and measuring necessary parameters of bubble images were also very crucial in order to investigate the behavior of laser induced bubbles. Therefore, MATLAB 2016a software tool was used to process bubble images, because it has various image processing functions in addition to its fast and robust structure. Different image processing functions in MATLAB were enabled to verify processed image features. Recorded videos were imported to MATLAB workspace, after the recordings of bubbles were taken each frame was processed with a digital image processing algorithm developed in MATLAB.

3.2 Image Capturing

This study includes analysis of bubble images that are captured by three different imaging systems. In each step, imaging system is improved in order to provide better conditions for evaluating bubble pictures.

3.2.1 CCD Camera Images

The specifications of CCD camera are discussed in section 3.1.3, but its performance was not shared in that section. CCD camera has 5X zoom capacity and has frame rate of maximum 30 fps. However, laser induced bubbles are

formed in nanoseconds and rise up in milliseconds. Therefore, it was very hard to capture laser induced bubbles with this camera, because its shutter speed was not fast enough to capture bubbles spherical shape without any distortion. Additionally, laser induced bubble size was around 30-40 micrometer, so bubbles covered only 5-6 pixels in captured images because of zoom capacity of camera. Figure 3.2.1.1 shows a sample image of laser induced bubble that was captured with this camera.

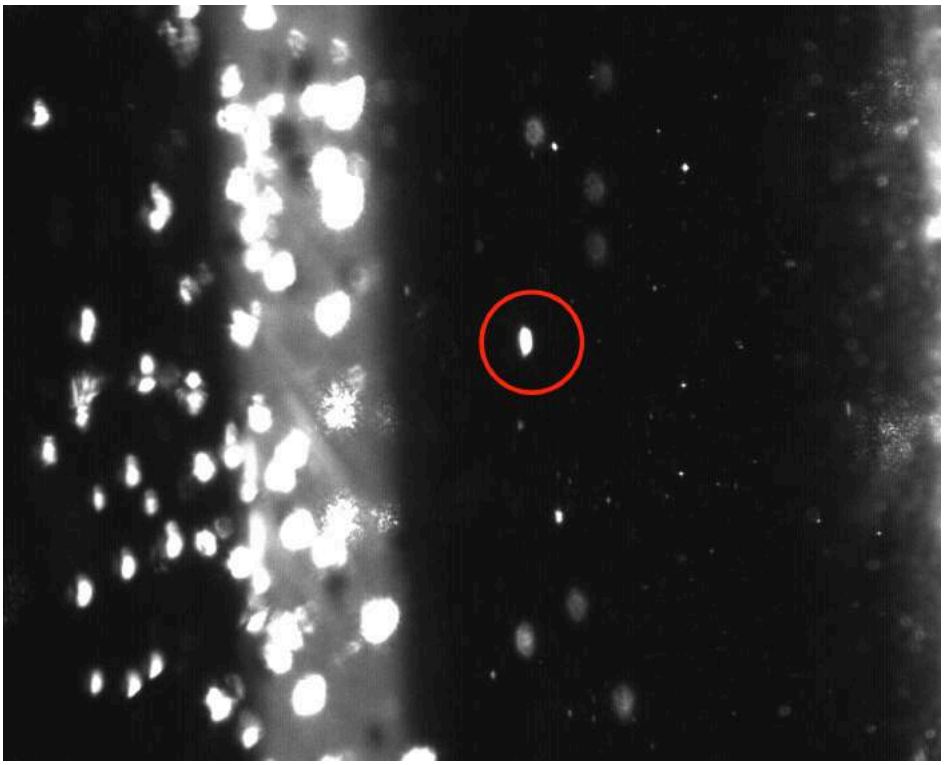

Figure 3.2.1.1 A sample image that was taken with the CCD camera. Fluid enlightened by the slit light to let bubbles glow. Glowing bubble is encircled with a red circle.

Bubble appeared very small and elliptic in images because camera magnification was limited to 5X zoom and the shutter speed was not fast enough to capture bubbles without any distortion. In this range of quality, it was unlikely to observe difference between bubbles, because exact shapes of bubbles could not be captured with this camera. Despite the failure of accurate imaging of bubbles, images that were taken with this system, were used to understand how bubbles volume changed as they rose in the fluid. These images helped us to understand

how much diffusion occurs between the gas inside of bubble and fluid, while bubble was rising.

3.2.2 Digital Microscope Camera Images

The digital microscopic camera had much higher zooming capacity when compared to the CCD camera used in the first phase. It can zoom in up to 50X with optical zoom, additionally it can magnify objects with 10X digital zoom, which provides 500x zoom in total. This amount of magnification was enough to observe details of laser induced bubbles. However, even if it was specified as 30 fps filming rate in technical details, this camera could only take 10 frames per second in practice. Then, it replicated each frame two times and added them together. As a result, it created videos with 30 frames per second but only takes 10 frames in reality, which was an impossible for us to capture laser induced bubbles accurately. Figure 3.2.2.1 shows sample frames taken with the digital microscope camera and bubbles look very blurry and unclear. Since this camera has very high zoom, it can only display very small area. Because of its low frame rate, it could capture only 4 frames while laser induced bubble rose in the fluid.

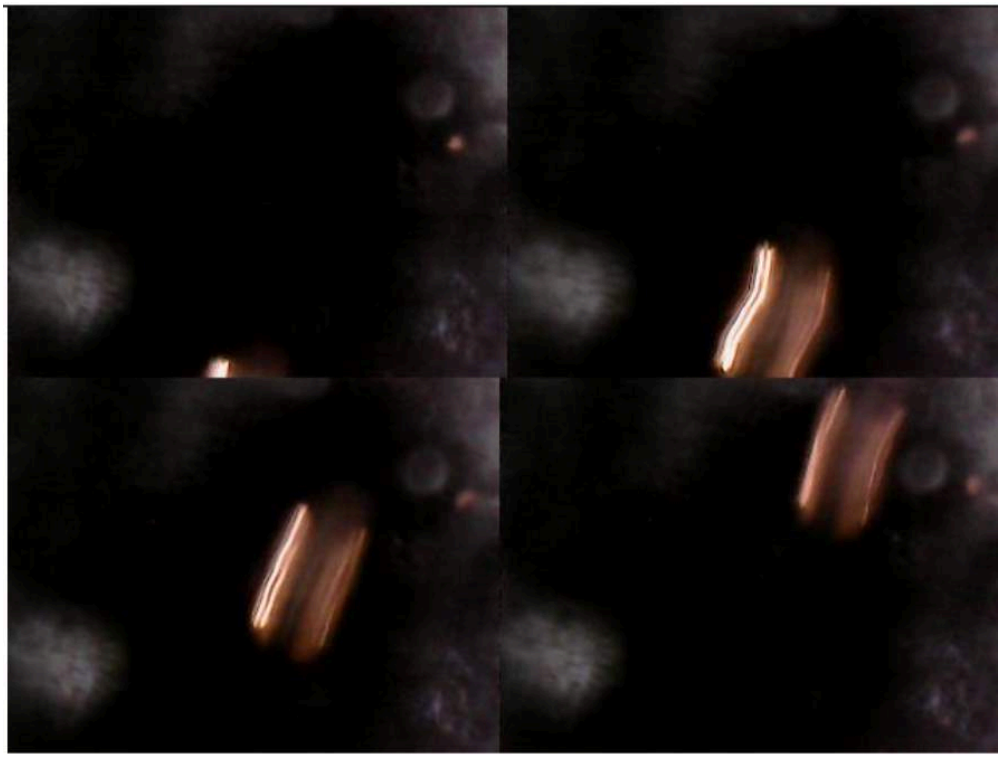

Figure 3.2.2.1 Digital microscope image samples prove the impossibility of capturing bubble images with this camera. Because of the low frame rate, drifted bubbles appeared in captured images.

3.2.3 Smartphone Camera Images

In this study, as it was mentioned before, a smart phone (iPhone 7) was used for recording slow motion videos of laser induced bubbles. However, iPhone 7 does not have optical zoom feature as default. Therefore, there was a need for an optic zoom lens in order to magnify the image, because the bubble sizes are in micrometer level. For this purpose, digital microscope is disassembled and its optical lens was taken off. Then this lens was integrated to our smartphone with the help of a silicon phone case. Figure 3.2.3.1 shows how lens and phone was integrated.

Figure 3.2.3.1 Lens is attached to the rear camera of our smartphone in order to provide an optic zoom to the camera. Lens is fixed with a silicon phone case.

With the lens attachment to the phone camera, it gained ability to magnify objects. This new feature was united with iPhone's slo-mo shooting option. It has become possible to record videos of laser induced bubbles in a reasonable magnification and fps rate. Figure 3.2.3.2 shows couple of frames of laser induced bubbles that were taken with this imaging system using our smartphone. In these frames a perfectly spherical shaped, large and clear laser induced bubble can be seen easily. Additionally, even it displayed very small area, it takes more than 200 frames of bubble before it went out from the viewfinder. Studies about improving imaging bubbles finished at this point because, requirements for the next steps of the study were substantially provided with this imaging technique.

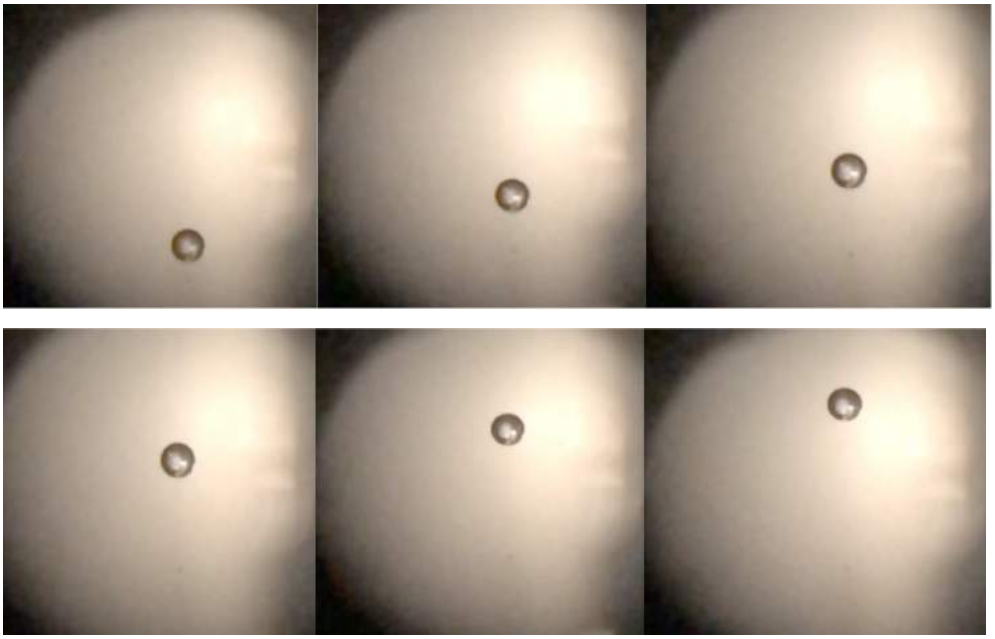

Figure 3.2.3.2 Sample images of a bubble that was captured with optic zoom lens attached smartphone camera. From left to right and top to bottom one can observe the rising of the bubble in the view.

3.3 Laser Induced Bubble Image Processing

Processing the captured images of laser induced bubbles followed the steps in figure 3.3.1. Different algorithms were used and developed in order to obtain meaningful parameters to understand bubble's characteristics.

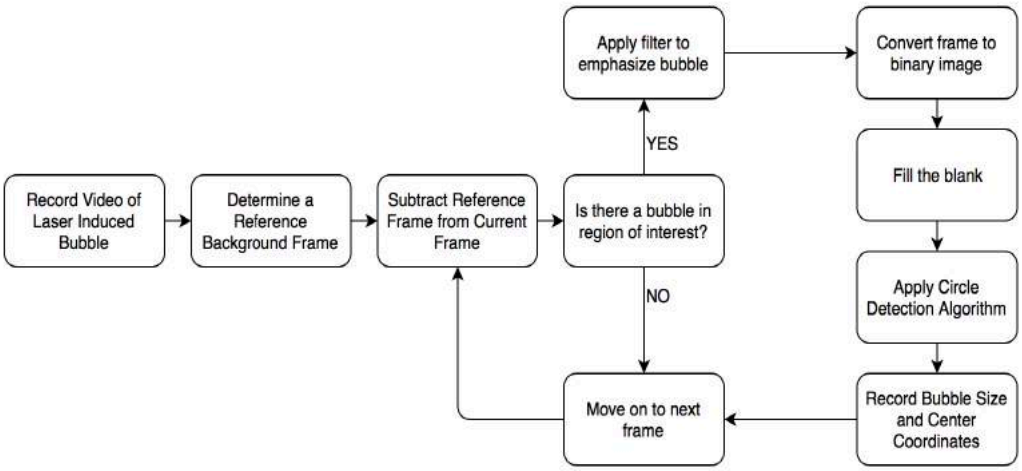

Figure 3.3.1 Algorithm details were briefly explained in this block diagram.

First, reference frame was chosen from the recording in order to get rid of all the constant objects and illumination in the record. Then, video recording was analyzed frame by frame. Each frame was taken and analyzed individually until the video ended. In every iteration of the algorithm, initially chosen reference frame was subtracted from the current frame. This operation created a single grey image which included only the difference between the current frame and reference frame. Figure 3.3.2 shows the same frame before and after reference frame subtracted. It also shows the reference frame. Choosing a reference frame played a critical role for the following steps. It had to be a very clear image that included only the background and illumination. Any other objects in the reference frame might have created unwanted results after it was subtracted from the current frame. Therefore, only constant elements should be included in the reference frame.

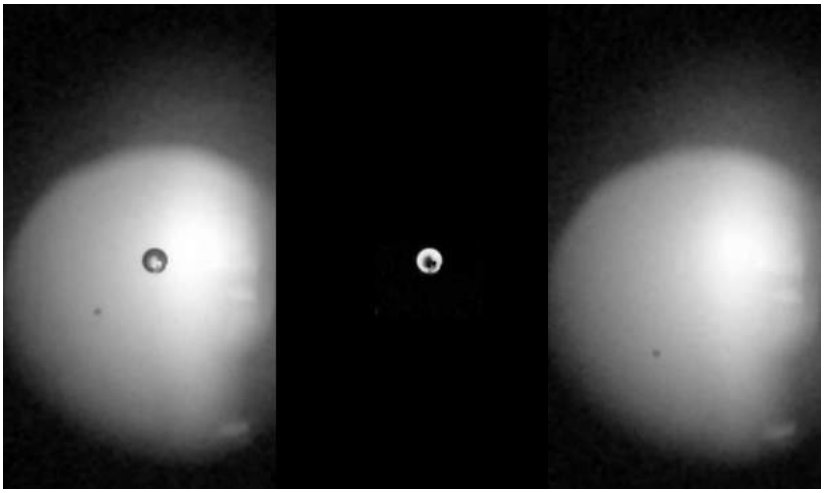

Figure 3.3.2 Captured raw image is showed on the left, in order to obtain the middle image reference image (the image on the right) was subtracted from the image on the left.

The subtracted image was then converted to a binary image in order to test if it contained any circular object in the region of interest. Since it was easier to perform morphological operations and detection algorithms on binary image, grey to binary conversion was preferred. After that, testing was completed by checking if the number of circular object's white pixels exceeded an expected threshold value in the region of interest. If the answer was yes, then circle detection algorithms were applied. But if the answer was no, algorithm moved on to the next frame. Thanks to this operation, the execution of the algorithm saved significant time by not applying further operations on frames that did not contain any bubbles in the region of interest.

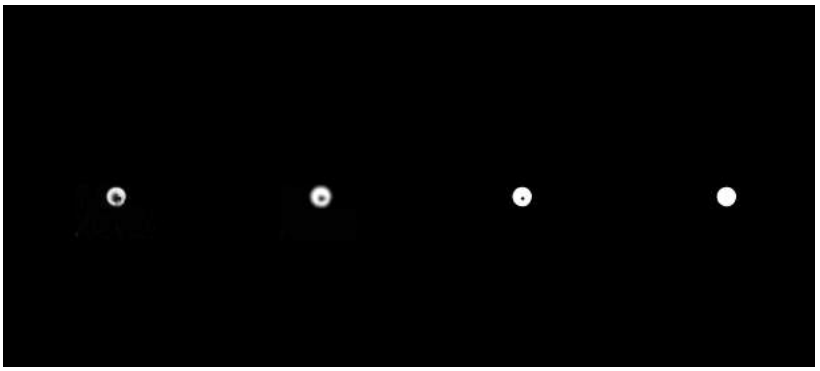

Figure 3.3.3 First image from the left shows the bubble image after the reference image was subtracted. After thresholding and circular filtering, second image from the left was obtained. Third image from the left shows the gray to binary conversion. Hole inside the bubble was filled as it is shown on the right-most image.

If there was a bubble presence in the region of interest, then algorithm started to apply series of morphological operations in order to detect exact boundaries of the bubble itself. First image was thresholded in order to highlight faded pixels of the bubble. Then, a circular filter is applied on the image that emphasized the circular objects which in this case is the bubble. However, the circular filter also blurred the boundaries of the object which can be seen in figure 3.3.3.

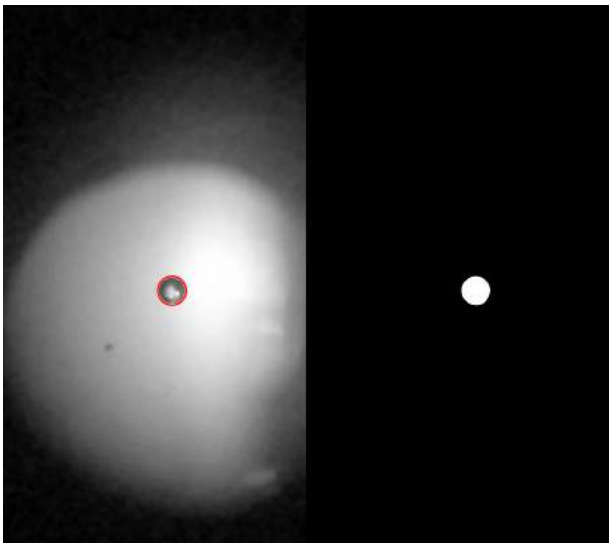

Figure 3.3.4 Circle detection algorithm was executed over the binary image on the right. Detected circle was drawn on the actual image (left) with a bubble in order to show how good it fitted.

Filtered image was taken into grey to binary image converter function, threshold level for choosing 0 or 1 for each pixel, was decided based on the circular filter size. Only pixels where bubble was present took value 1 and the rest took zero value in this new binary image. If there was a hole in the bubble, it was filled by morphological dilation. This new binary image was taken into the circle detection algorithm, which is a built-in function in MATLAB. This function takes the image, applies the Hough transform based circular detection algorithm, and fits the smallest circle that can cover the white region in the image. Then, it gives detected circle's center coordinates and radius as an output if it detects any. If it does not detect any circular object it gives empty matrix as an output. Figure 3.3.4 shows a detected and fitted circle that is plotted on an actual frame.

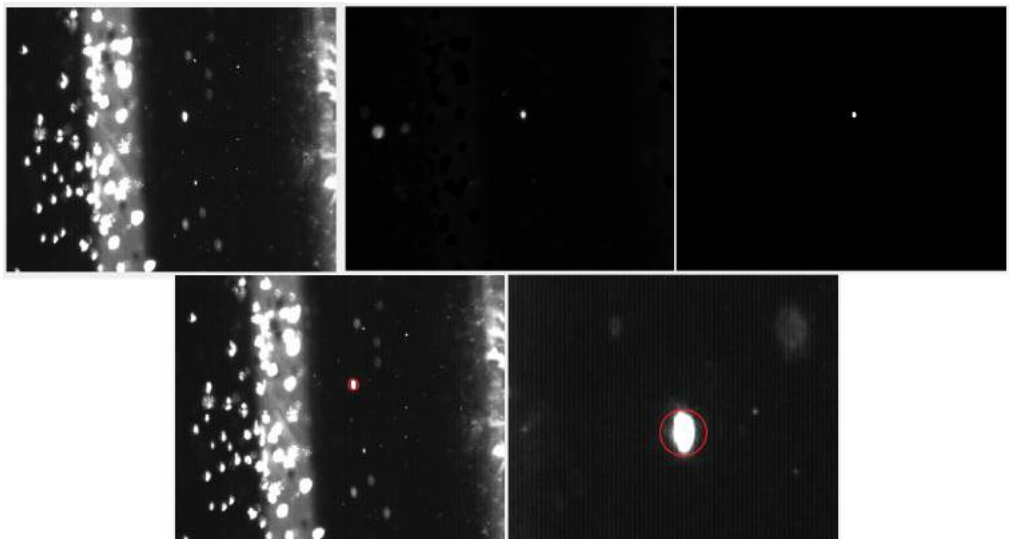

Figure 3.3.5 Images that were captured with the CCD camera, were processed with this algorithm. Those images show important steps of the image outputs. Last image shows fitted circle to a bubble. Since captured images were not good, circles did not fit perfectly.

The last step of bubble detection algorithm, before it moved on to the next frame, was recording the center coordinate values and radius value of the bubble in a matrix. This helped us to look at each bubble's behavior for a certain amount of time. It was also possible to analyze how bubble volume changed while it was rising, and how it was moving to the top in different fluids. Figures 3.3.5 and 3.3.6 show clearly each step of how one frame was processed. Figure 3.3.5 shows images recorded by the CCD camera, and it can be seen that bubbles appear very small. However, bubbles are clear and larger in figure 3.3.6.

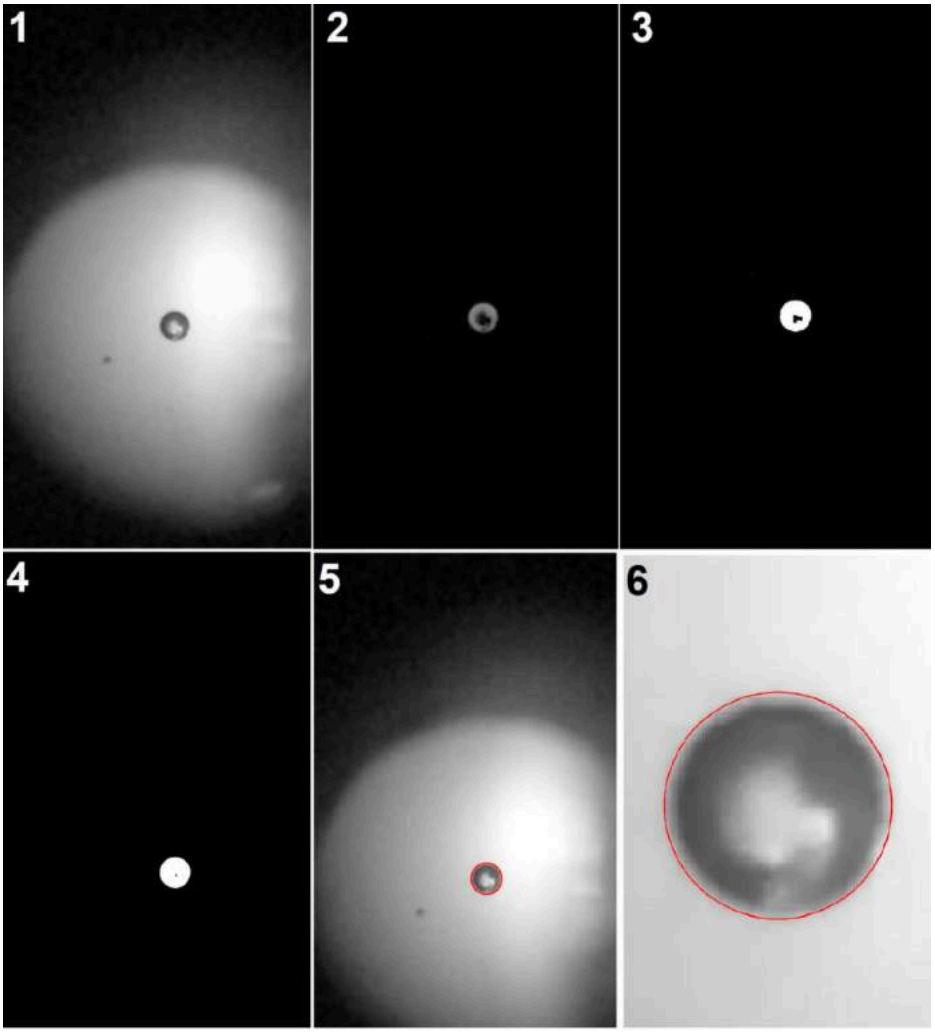

Figure 3.3.6 Image that were captured with the smartphone and lens, were processed with the algorithm whose steps were summarized over these six images.

3.4 Fluid Effects on Bubble

Two different fluids were used in this study and their effects on laser induced bubbles were investigated. Main difference between two fluids (water and baby oil) that were used in this study, were their density. Different density values effect laser induced bubbles differently. The reason of this is related to laser induced bubble physics [10]. It is shown in many studies that fluid density effects the maximum radius size of the first occurred laser induced bubble [8]–[10], [12],

[38]. This means, higher fluid density reduces maximum radius value that bubble can reach.

$$F = \rho \times g \times V \tag{3.4.1}$$

Also, higher density means higher buoyancy according to Archimedes' law which means bubbles rise up faster in fluids which have higher density.
In this study water have higher density, therefore observed laser induced bubbles appeared a little smaller and rose faster in the water. On the other hand, laser induced bubbles appeared bigger and rose slowly in baby oil because of the lower buoyancy, which allowed us to capture better bubble images in baby oil.

3.5 Configurable Pressure System

Configurable pressure system was the last step of our experimental setup. It was important to configure the pressure level systematically in order to investigate how laser induced bubble behavior changes for different pressure levels. Thus, in order to create this system where fluid pressure systematically configured, fluid was filled to a silicon tube. Then, one end of this tube was connected to the glass cuvette and the other end was connected to fluid container. Leak-proof glass cuvette was filled with fluid and was disengaged from the air. Figure 3.5.1 and 3.5.2 show the theoretical and the actual setup, respectively.

$$P = h \times \rho \times g \tag{3.5.1}$$

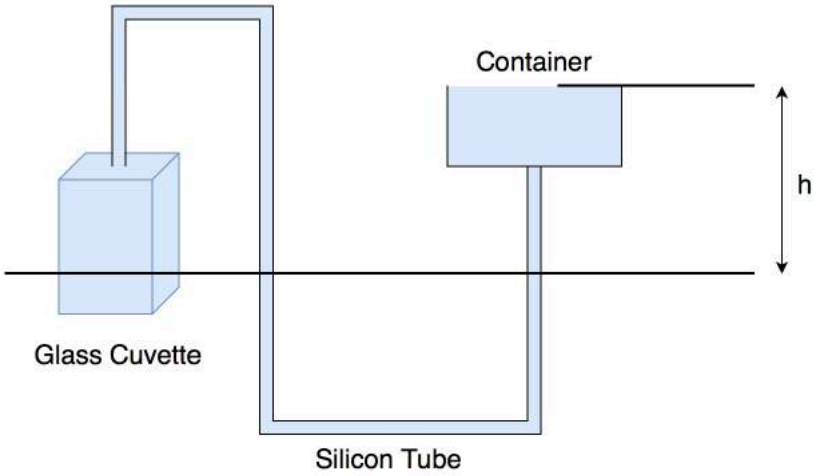

Figure 3.5.1 Pressure of fluid inside the glass cuvette was determined by changing the h value, which is shown here.

This setup ensured that fluid pressure in glass cuvette would only depend on the height of the fluid. This pressure can be calculated with Pascal's law. By changing height of the container, fluid pressure in cuvette can be determined.

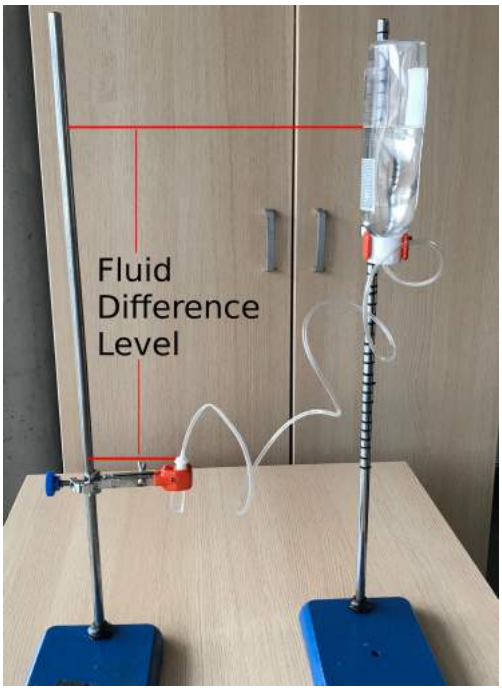

Figure 3.5.2 Pressure of the fluid inside the glass cuvette depends on the fluid difference level.

Chapter 4

Results and Discussion

In this chapter, experimental results are shared and discussed. In order to understand laser induced bubble behavior, different experiments were performed. Three parameters were changed to understand how bubble behaviors change. These parameters were the energy level adjusted to generate laser pulses, the density of the fluid in which the bubbles were formed, and the fluid pressure.

4.1 Laser Energy Effect

Short pulse laser energy focused at a point in the fluid causes formation of plasma at that point, and vaporization of the fluid to eventually result in a bubble in the fluid. However, there is no certain threshold energy value for triggering this action. The first parameter that is investigated in this experiment was the laser energy. In order to understand the effect of laser energy, different energy levels were used to generate the laser induced bubbles. To perform this analysis, the initial energy level of 0.8 mJ was selected. It was possible to adjust the energy level using the user interface of the laser system. At each energy level, multiple (up to 20) shots were applied most of which resulted in bubble formation. For each bubble, using the imaging system and software, the area (measured with the number of white pixels) corresponding to that bubble was computed. Average area value was computed using all the bubbles formed at each energy level. After 0.8 mJ, the energy levels were set at 1.0, 1.2, and 1.4 mJ and similar procedure was followed.

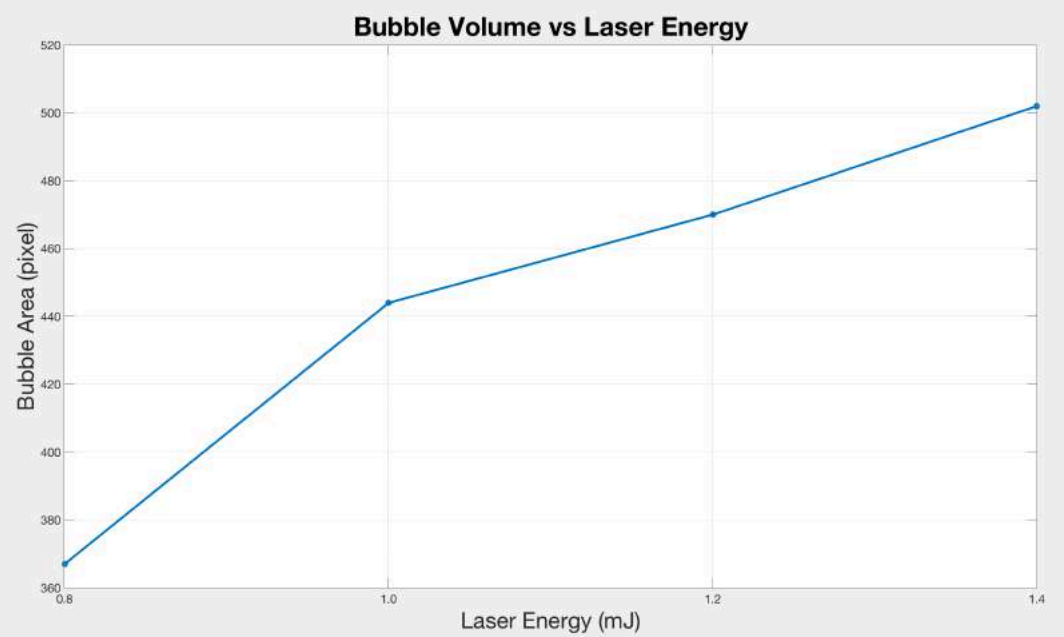

Figure 4.1.1 This figure shows how bubble volume changes with increasing laser energy.

Figure 4.1.1 shows how bubble volume (total number of white pixels=bubble area was related to the bubble volume) changes at different energy levels. It was expected that the bubble volume should increase with the increase in the amount of applied energy. Experiments indicated that the minimum required energy for creating a bubble is about 0.6 mJ. However, it was better to apply a little higher energy to obtain identical bubbles, because laser core might not deliver the same energy level at all times. It is known that the laser core sometimes cannot deliver the same energy in serial laser shots. For instance, if the laser was set to 1 mJ energy level, during the serial laser shots, some of the shots contained 0.95 mJ energy and some others contained 1.05 mJ energy. This deviation might have prevented creating identical bubbles at the minimum energy level (0.6 mJ).

One of the observations we had in the experiments was that increased laser energy caused some of the laser bubbles to fragment into a couple of smaller-size bubbles. The reason of this behavior can be explained with the shockwaves emitted after the first collapse. Increased energy caused emitting more powerful shockwaves which can split bubble into a couple of smaller-size bubbles. Figure 4.1.2 shows laser induced bubbles that were created with different energy levels.

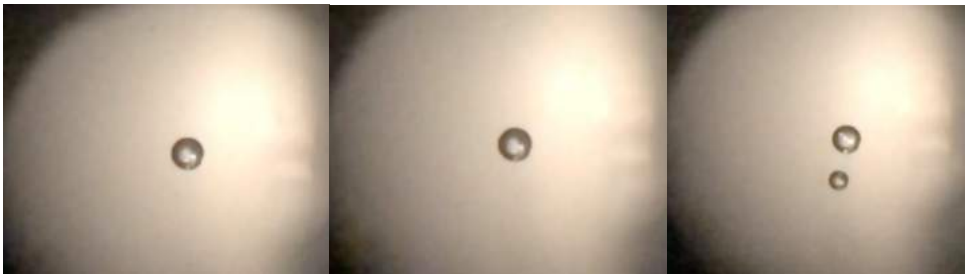

Figure 4.1.2 Bubbles that are created with different laser energy levels are showed. Bubble in the left image created with 1mJ laser energy. Bubble in the middle image created with 1.2 mJ laser energy and bubbles in the right image created with 1.5 mJ. It can be seen that couple of bubbles appeared when laser energy increased.

It was also observed that in higher energy levels more than one bubbles occurred instead of a single bubble. Optimum laser energy to create single laser induced bubbles was chosen as 1mJ, because in lower values some shots did not result in any bubbles due to the variance in laser core energy. Moreover, higher energy values created more than one bubble which was an unwanted situation for this study. However, it was concluded that the energy level of 1 mJ prevented those disadvantages, because it was still very likely to produce bubbles with slightly lower energy than 1 mJ. Also, it was unlikely to produce more than one bubble with slightly more energy than 1 mJ. Therefore, laser shots with 1 mJ energy level always produced a single bubble as it was aimed.

4.2 Fluid Effect

In this study as it was discussed in the previous chapter, two different fluids were used for imitating the intraocular environment. Pure water was used in the early stages of the study, because its density is closer to the humor aqueous. However, multiple bubbles often occurred in pure water and this created a disadvantage for investigating the bubble behavior. Therefore, instead of using pure water, commercially available baby oil was used in further stages of the study. Baby oil has lower density than water which allowed us to create a single bubble easier than it was in water. It was a better option in order to carry out the proof of concept

work that was proposed in this study. In addition to that, laser induced bubbles rose slowly in baby oil which made it easier to track them with our imaging system and software.

4.3 Pressure Effect

The most important milestone of this study was to prove that the laser induced bubbles' volume changed corresponding to the fluid pressure. Theoretically, it was proposed that the bubble volume would decrease with increasing fluid pressure. Our experiments showed that this was true. In section 3.5, the experimental setup used in this study, shown in figure 4.3.1, was explained in a detailed manner.

Figure 4.3.1 Experiment setup with imaging system.

Experiments were performed with different pressure levels starting from 0 mmHg to 6 mmHg pressure. In each step, the pressure level was increased by 2 mmHg. Single laser induced bubbles were created and recorded multiple times for each pressure level. Then, recorded videos were processed as it was discussed in section 3.3. In order to calculate the volume of laser induced bubbles from the extracted information of their center coordinates and radii, two methods were used. First, bubble radii were employed to calculate their volumes with equation 4.3.1.

$$V = {}^{4}/_{3} \times \pi \times r^{3} \tag{4.3.1}$$

Computations were performed for each bubble at each pressure level. Then, the results were averaged for each pressure level. Figure 4.3.2 shows the averaged volume values at each pressure level.

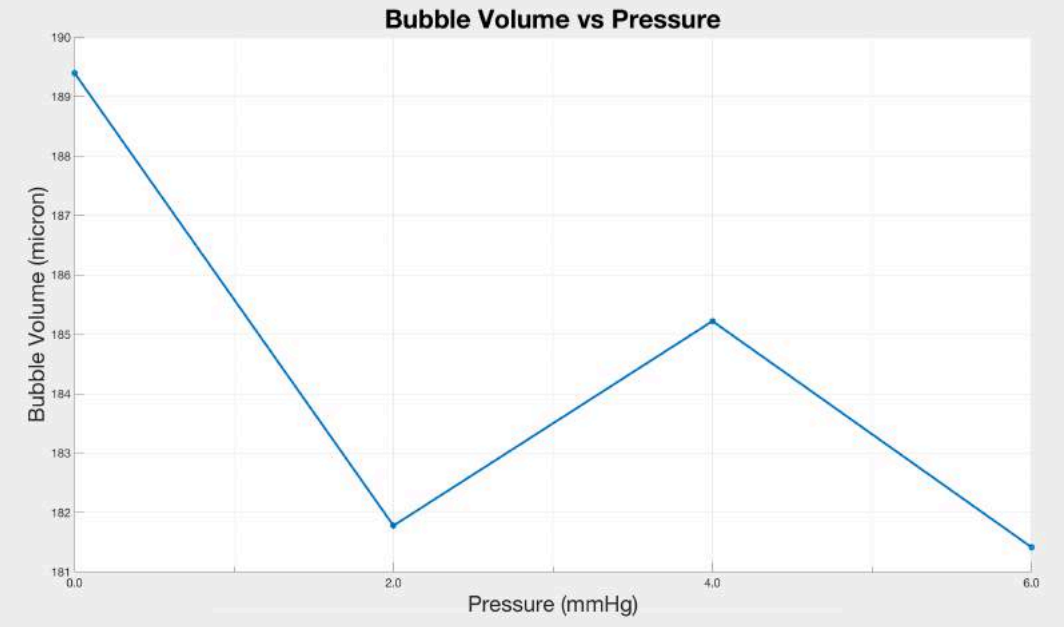

Figure 4.3.2 Volume estimation using fitted circles' radii gave misleading results about the bubble volumes.

Results that were obtained using the radius values did not show an exact correlation between volume and pressure. Because, bubble radius values varied even for the bubbles that were formed at the same pressure level. The reason of

this variance was the movements of laser induced bubbles after they were formed. Figure 4.3.3 shows how laser induced bubbles move after they are created.

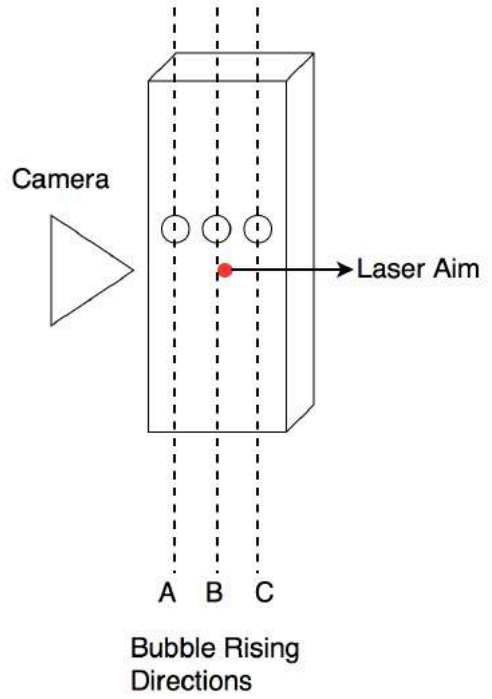

Figure 4.3.3 Bubble motion inside of glass cuvette. If a bubble passed through A direction, its radius appeared larger in images. If a bubble passed through B or C its radius appeared smaller than A direction.

All laser induced bubbles rose up, but their location on x-y plane differed and if they were closer to the imaging system, their radii were measured larger. If they were further away from the imaging system, then their radii were measured smaller. This caused the variance between bubble sizes computed with the algorithm.

The variance of radius values of bubbles at the same pressure level led us to find another method to compute bubble volumes. Therefore, another approach was developed to solve this problem. The volume was one of the components of lifting force equation of Archimedes which was discussed in section 3.4. Therefore, the idea of the second approach was first calculating the lifting force that was applied on the bubbles. This was possible by calculating the bubbles' rising speed. Then from lifting force, volume values could be calculated. Since circle detection

algorithm provided the coordinate values of the center of the detected circles, the rising speed of a bubble could be calculated. The y coordinate changes in the bubbles in each frame could be differentiated to obtain the rising speed of the bubble. Those speed values were averaged to get an average speed of each individual bubble. After this point, the volume value could be derived from the Archimedes' Law as given in equation 4.3.2.

$$V = \frac{F}{\rho \times g} = \frac{m \times a}{\rho \times g} \tag{4.3.2}$$

This approach provided more reliable results. While small changes of radius value affected volume computations dramatically, center coordinates of the bubble did not alter too much even if they moved closer to or further away from the imaging system. Thus, derived volume values from rising speed of bubbles provided more accurate results. Figure 4.3.4 shows the second approach's results demonstrating the relationship between the pressure in the fluid and the bubble volume. This depicted that the laser induced bubble volumes changed depending on the fluid pressure level.

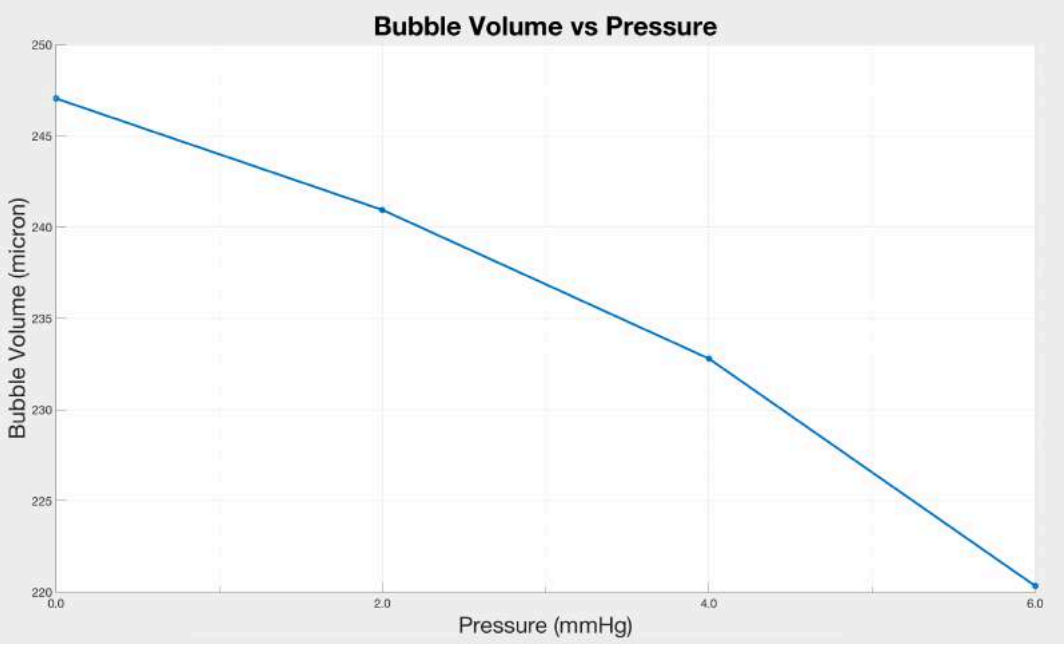

Figure 4.3.4 Bubble volume estimation with using bubbles rising speed gave more reliable results about bubble volumes.

Figure 4.3.5 also shows the comparison of computed volume values of the first and the second approach. From this figure, it is obvious that speed based approach gave more reliable results than the radius based approach.

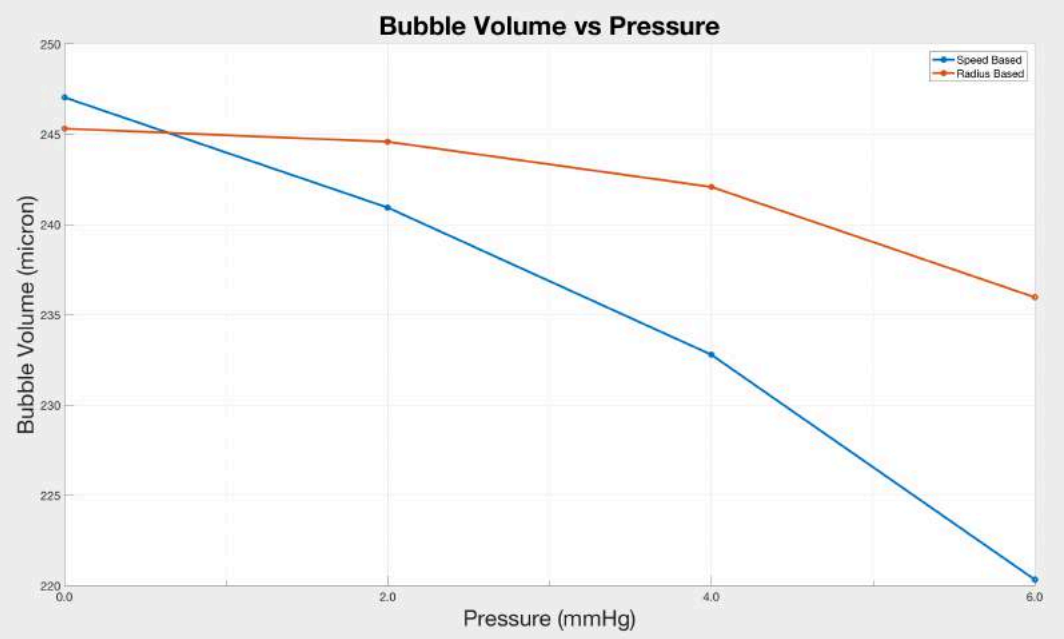

Figure 4.3.5 Comparison of two methods for bubble volume computation. Blue line shows the volume estimation that uses speed of rising bubbles. Red line shows radius based estimation results.

4.4 Dead Animal Eye Experiments

After the proof of concept stage was complete, our experiments were focused on measuring laser induced bubble volumes in real intraocular environments. For this purpose, dead animal eyes were used. Dead sheep eyes were bought from a butcher's shop and used in the experiments. Sheep eyes are bigger and have more convex structure then human eyes, which provided more comfortable workspace for imaging system. However, dead eye's cornea rapidly loses its transparent structure starting from the center of the cornea, which makes it impossible to perform laser shots aiming straight to the center of the anterior chamber. The portion of the eye where cornea and sclera meet can keeps its transparency for a

couple of hours. Thus, it was possible to create laser induced bubbles in this area of the anterior chamber. Figure 4.4.1 shows several laser induced bubbles formed in the eye of a dead sheep.

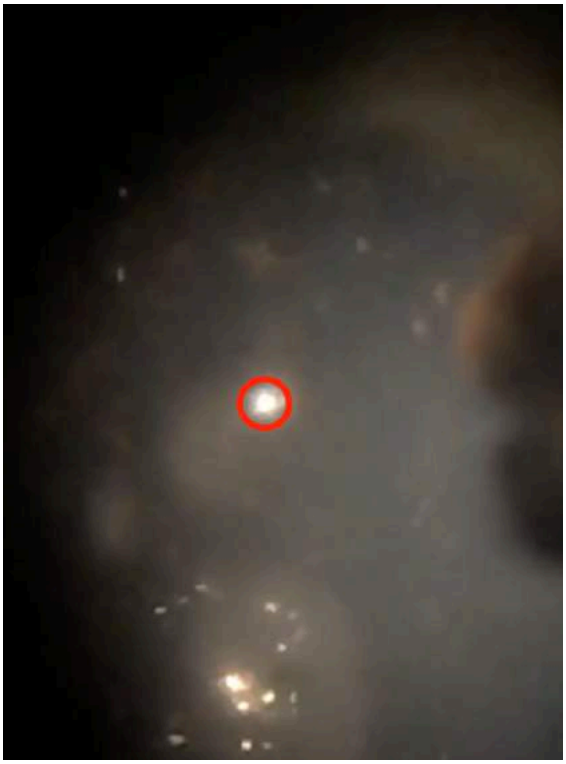

Figure 4.4.1 Bubble formed in a sheep eye is encircled with the red circle.

Even if the laser induced bubbles were created in dead animal eyes, upper area of the anterior chamber was very narrow and did not allow us to image the bubbles clearly from the side. This prevented us to record a clear video of the bubbles and compute their volumes. This stage was the final stage of our study, and such inefficient conditions prevented us to perform experiments on dead animal eyes.

Chapter 5

Conclusion

This study aimed to perform a preliminary work in solving the problem of measuring intraocular pressure that ophthalmology clinicians have been encountering frequently. It is important to note that this was a proof-of-concept study to examine the idea that it is possible to measure the intraocular pressure using laser induced bubbles, which are created in the anterior chamber of the eye. This study was inspired from the behaviors and characteristics of laser induced bubbles in fluids.

Available tonometers measure the change of resilience of cornea or sclera in order to estimate intraocular pressure. However, resilience depends on the thickness and corrosion besides the intraocular pressure. Thus, these tonometers cannot measure intraocular pressure precisely, and sometimes the measured values should be corrected using a table that depends on the corneal thickness.

In this thesis study, it is proposed that the laser induced bubble volumes change depending on the fluid internal pressure. The amount of change in bubble volume might give information about the internal fluid pressure. In order to prove this concept, we have performed numerous experimental studies. Different parameters were changed in order to observe how these parameters affected the laser induced bubbles, their volume and movement characteristics. Fluid density, laser beam energy and internal fluid pressure are the three parameters that can affect laser induced bubble volume. In order to understand effect of internal fluid pressure, the other two parameters are stabilized and only internal fluid pressure is changed during the measurements. As reported in the Results and Discussion chapter, promising results were obtained from the experimental studies. The intuitive idea of this study was measuring the intraocular pressure by using laser induced

bubbles, thus all the measurements were taken from the experimental setup which imitated the intraocular environment. They showed that the fluid pressure had an effect on laser induced bubble volumes, and this volume-pressure relationship could be measured with the laser system and the imaging setup. Laser induced bubbles were created by Nd:YAG laser device that is already available for capsulotomy operations. Thus, any side effects of laser to cornea tissues can be predicted from previous studies on this area [2]. The precision of the measurements was 2 mmHg, and these measurements were not affected from any other parameters but the pressure. Due to the discussed technical limitations of laser device that is used in this study, more precise and more sensitive measurements could not taken, but at this point it is proved that the internal fluid pressure can be determined by measuring laser induced bubbles that are created in the fluid.

In the last step of this study, the proposed approach was tested on dead sheep eyes in order to investigate the feasibility of this approach in real intraocular environment. However, laser induced bubbles could not be generated and captured properly in the eye due to the opacification of dead cornea cells. Dead sheep eyes cornea lost its transparency starting from the center and became white in a very short time period, which made impossible to perform laser experiments on the dead sheep eye. Only side areas of cornea that intersects with sclera stayed transparent for couple hours. However, smartphone imaging system was unsuitable to visualize that cross-section area of the anterior chamber of the dead sheep eye. It can be only visualized from optical microscope of the Nd:YAG laser device and our imaging system was not compatible with the microscope. Thus, these limitations prevented to perform laser experiments on dead sheep eye.

Despite of all these limitations and drawbacks, this study proved that nature characteristics of laser induced bubbles regarding volume, correlates with fluid pressure. This most basic fact will be the base of our further studies about developing this measurement method for intraocular pressure. For this purpose, first imaging system will be redesigned to make it compatible with the optical microscope of the laser. Next, instead of dead sheep eye new alternatives will be

investigated for experimental usage such as live lab rabbit or lab rat eye and needed ethical committee permissions will be obtained. Further studies with these improvements will show whether this method can substitute the current methods of measuring intraocular pressure, but the results of this study strongly promise that usage of laser induced bubbles for measuring intraocular pressure is applicable.

BIBLIOGRAPHY

[1] F. Buratto, L; Brint; Stephen, *LASIK Principles and Techniques*. Slack, 1998.

[2] M. G. Kerr Muir and E. S. Sherrard, "Damage to the corneal endothelium during Nd/YAG photodisruption.," *Br. J. Ophthalmol.*, vol. 69, no. 2, pp. 77–85, 1985.

[3] C. A. Puliafito and R. F. Steinert, "Short-Pulsed Nd:YAG Laser Microsurgery of the Eye: Biophysical Considerations," *IEEE J. Quantum Electron.*, vol. 20, no. 12, pp. 1442–1448, 1984.

[4] A. Vogel, W. Hentschel, J. Holzfuss, and W. Lauterborn, "Cavitation Bubble Dynamics and Acoustic Transient Generation in Ocular Surgery with Pulsed Neodymium:YAG Lasers," *Ophthalmology*, vol. 93, no. 10, pp. 1259–1269, 1986.

[5] K. E. Han, H. Kim, N. R. Kim, I. Jun, E. K. Kim, and T. I. Kim, "Comparison of intraocular pressures after myopic laser-assisted subepithelial keratectomy: Tonometry-pachymetry, Goldmann applanation tonometry, dynamic contour tonometry, and noncontact tonometry," *J. Cataract Refract. Surg.*, vol. 39, no. 6, pp. 888–897, 2013.

[6] J. Sánchez-Navés, L. Furfaro, O. Piro, and S. Balle, "Impact and permanence of LASIK-induced structural changes in the cornea on pneumotonometric measurements: contributions of flap cutting and stromal ablation.," *J. Glaucoma*, vol. 17, no. 8, pp. 611–8, 2008.

[7] P. G. Mardelli, L. W. Piebenga, M. M. Whitacre, and K. D. Siegmund, "The effect of excimer laser photorefractive keratectomy on intraocular pressure measurements using the Goldmann applanation tonometer.," 1997.

[8] K. T. Byun and H. Y. Kwak, "A Model of Laser-Induced Cavitation," *Japanese J. Appl. Physics, Part 1 Regul. Pap. Short Notes Rev. Pap.*, vol. 43, no. 2, pp. 621–630, 2004.

[9] C. E. Brennen, *Cavitation and Bubble Dynamics*. Cambridge University Press, 2013.

[10] W. Lauterborn and C. D. Ohl, "Cavitation bubble dynamics," *Ultrason. Sonochem.*, vol. 4, no. 2, pp. 65–75, 1997.

[11] I. Akhatov, O. Lindau, A. Topolnikov, R. Mettin, N. Vakhitova, and W. Lauterborn, "Collapse and rebound of a laser-induced cavitation bubble," *Phys. Fluids*, vol. 13, no. 10, pp. 2805–2819, 2001.

[12] X. D. Ren *et al.*, "Experimental investigation on dynamic characteristics and strengthening mechanism of laser-induced cavitation bubbles," *Ultrason. Sonochem.*, vol. 32, pp. 218–223, 2016.

[13] N. Bloembergen, "Laser Induced Electric Breakdown in Solids," *IEEE J. Quantum Electron.*, vol. 10, no. 3, pp. 375–386, 1974.

[14] P. A. Quinto-Su, V. Venugopalan, and C.-D. Ohl, "Generation of laser-

induced cavitation bubbles with a digital hologram.," *Opt. Express*, vol. 16, no. 23, pp. 18964–18969, 2008.
[15] P. K. Kennedy, D. X. Hammer, and B. A. Rockwell, "Laser-induced breakdown in aqueous media," *Prog. Quantum Electron.*, vol. 21, no. 3, pp. 155–248, 1997.
[16] "Glaucoma Research Foundation." [Online]. Available: https://www.glaucoma.org/glaucoma/anatomy-of-the-eye.php. [Accessed: 30-Nov-2017].
[17] L. A. Marzette and L. W. Herndon, "Glaucoma risk factors: The cornea," in *Clinical Glaucoma Care: The Essentials*, 2014, pp. 29–43.
[18] M. R. Wilson and M. Gallardo, "Glaucoma risk factors: Ethnicity and glaucoma," in *The Glaucoma Book: A Practical, Evidence-Based Approach to Patient Care*, 2010, pp. 101–109.
[19] N. A. Loewen and A. P. Tanna, "Glaucoma risk factors: Intraocular pressure," in *Clinical Glaucoma Care: The Essentials*, 2014, pp. 1–22.
[20] T. Juhasz, G. A. Kastis, C. Suárez, Z. Bor, and W. E. Bron, "Time-resolved observations of shock waves and cavitation bubbles generated by femtosecond laser pulses in corneal tissue and water," *Lasers Surg. Med.*, vol. 19, no. 1, pp. 23–31, 1996.
[21] J. G. Fujimoto, W. Z. Lin, E. P. Ippen, C. A. Puliafito, and R. F. Steinert, "Time-resolved studies of Nd:YAG laser-induced breakdown: Plasma formation, acoustic wave generation, and cavitation," *Investig. Ophthalmol. Vis. Sci.*, vol. 26, no. 12, pp. 1771–1777, 1985.
[22] G. Toker, V. Bulatov, T. Kovalchuk, and I. Schechter, "Micro-dynamics of optical breakdown in water induced by nanosecond laser pulses of 1064 nm wavelength," *Chem. Phys. Lett.*, vol. 471, no. 4–6, pp. 244–248, 2009.
[23] M. P. Felix and A. T. Ellis, "Laser-induced liquid breakdown-a step-by-step account," *Appl. Phys. Lett.*, vol. 19, no. 11, pp. 484–486, 1971.
[24] F. Docchio, P. Regondi, M. R. Capon, and J. Mellerio, "Study of the temporal and spatial dynamics of plasmas induced in liquids by nanosecond Nd:YAG laser pulses. 1: Analysis of the plasma starting times.," *Appl. Opt.*, vol. 27, no. 17, pp. 3661–8, 1988.
[25] C.-D. Ohl, T. Kurz, R. Geisler, O. Lindau, and W. Lauterborn, "Bubble dynamics, shock waves and sonoluminescence," *Philos. Trans. R. Soc. A Math. Phys. Eng. Sci.*, vol. 357, no. 1751, pp. 269–294, 1999.
[26] C. B. Schaffer, N. Nishimura, E. N. Glezer, A. M.-T. Kim, and E. Mazur, "Dynamics of femtosecond laser-induced breakdown in water from femtoseconds to microseconds," *Opt. Express*, vol. 10, no. 3, p. 196, 2002.
[27] A. Tomita, Y. and Shima, "High-speed photographic observations of laser-induced cavitation bubbles in water," *Acta Acust. united with Acust.*, vol. 71, pp. 161--171, 1990.
[28] W. Lauterborn, "High-speed photography of laser-induced breakdown in liquids," *Appl. Phys. Lett.*, vol. 21, no. 1, pp. 27–29, 1972.
[29] A. Vogel, S. Busch, K. Jungnickel, and R. Birngruber, "Mechanisms of

intraocular photodisruption with picosecond and nanosecond laser pulses," *Lasers Surg. Med.*, vol. 15, no. 1, pp. 32–43, 1994.
[30] A. Vogel, S. Busch, and U. Parlitz, "Shock wave emission and cavitation bubble generation by picosecond and nanosecond optical breakdown in water," *J. Acoust. Soc. Am.*, vol. 100, no. 1, pp. 148–165, 1996.
[31] F. R. Gilmore, "The Growths or Collapse of a Spherical Bubble in a Viscous Compressible Liquid," 1952.
[32] W. Lauterborn and A. Vogel, "Shock wave emission by laser generated bubbles," in *Bubble Dynamics and Shock Waves*, 2013, pp. 67–103.
[33] E.-A. Brujan, K. Nahen, P. Schmidt, and A. Vogel, "Dynamics of laser-induced cavitation bubbles near an elastic boundary," *F. Fluid Mech.*, vol. 433, pp. 251–281, 2001.
[34] A. Vogel and W. Lauterborn, "Acoustic transient generation by laser-produced cavitation bubbles near solid boundaries," *J. Acoust. Soc. Am.*, vol. 84, no. 2, pp. 719–731, 1988.
[35] W. D. Song, M. H. Hong, B. Lukyanchuk, and T. C. Chong, "Laser-induced cavitation bubbles for cleaning of solid surfaces," *J. Appl. Phys.*, vol. 95, no. 6, pp. 2952–2956, 2004.
[36] C. D. Ohl, M. Arora, R. Dijkink, V. Janve, and D. Lohse, "Surface cleaning from laser-induced cavitation bubbles," *Appl. Phys. Lett.*, vol. 89, no. 7, 2006.
[37] M. S. Hutson and X. Ma, "Plasma and cavitation dynamics during pulsed laser microsurgery in vivo," *Phys. Rev. Lett.*, vol. 99, no. 15, 2007.
[38] Lord Rayleigh, "VIII. On the pressure developed in a liquid during the collapse of a spherical cavity," *Philos. Mag. Ser. 6*, vol. 34, no. 200, pp. 94–98, 1917.

APPENDIX

MATLAB Code

```
clc;
clear all;

%-- Read video and record it to variable v
v = VideoReader('bubble_video.MOV');

%-- Calculate total number of frame for initialization
max_index_of_frame = ceil(v.FrameRate*v.Duration);

%-- Initialization of parameters
current_frame = cell(1,max_index_of_frame);
smalldif = cell(1,max_index_of_frame);
dif = cell(1,max_index_of_frame);
total_numberof_pixels = zeros(1,max_index_of_frame);
radii_s = cell(1,max_index_of_frame);
centers_s = cell(1,max_index_of_frame);

i = 1;      %-- Counter for indexing
vis = 0;    %-- On/Off switch for plotting

%-- First frame of video taken as reference
fullbase = rgb2gray(readFrame(v));

%-- ROI for detecting bubble presence
mask1 = zeros(1280,720); mask1(670:788,260:520) = 1;
%-- ROI for detecting circle and fitting circle to bubble
mask2 = zeros(1280,720); mask2(630:828,260:540) = 1;

h = fspecial('disk',10);    %-- Circular image dilation filter

while hasFrame(v)           %-- Starts reading frames of video

    tempf = readFrame(v);
    current_frame{i} = tempf;
    current_frame{i} = rgb2gray(current_frame{i}); %-- Convert to gray

    if i < 6
        %-- Defines average background to detect if bubble passes from ROI
        baseframe = baseframe + current_frame{i}(670:788,260:520)/5;
    end;

    %-- Find difference between current frame and baseframe
    %-- Apply medfilt to clear noise
    smalldif{i} = imabsdiff(baseframe,current_frame{i}(670:788,260:520));
    smalldif{i} = medfilt2(im2bw(smalldif{i},0.07),[10 10]);

    %-- Count total white pixels (the difference)
    total_numberof_pixels(i) = sum(sum(smalldif{i}));

    if total_numberof_pixels(i) > 1200  %-- Threshold for bubble presence

        %-- If this frame is the first frame that bubble entered ROI
        if total_numberof_pixels(i-1) < 1200
            %-- Update fullbase by taking average of 5 frames that is
            %   exactly 1 second before the current frame
            fulbase = (current_frame{i-32}+current_frame{i-31}...
                +current_frame{i-30}+current_frame{i-29}+...
                current_frame{i-28})/5;
```

```
        end;

        %-- Find difference of current frame from updated fullbase which
        %   shows bubble presence
        dif{i} = uint8(mask2).*imabsdiff(fullbase,current_frame{i});

        %-- Amplify pixel values in order to clear diffence between bubble
        %   and background
        dif{i}(dif{i}>30) = 255;

        %-- Apply circular filter to highlight circular objects, then apply
        %   median filter to clear out noise, finally apply black&white
        %   transformation to frame.
        dif{i} = imfilter(dif{i},h);
        dif{i}(dif{i}>130) = 255;
        dif{i} = im2bw(medfilt2(dif{i},[15 15]),0.9);

        %-- Detect circular objects in current binary frame
        stats = regionprops('table',dif{i},'Centroid',...
            'MajorAxisLength','MinorAxisLength');

        %-- Diameters along x and y axis are extracted and radiis values
        %   are calculated. Also, center coordinates are extracted
        diameters = mean([stats.MajorAxisLength stats.MinorAxisLength],2);
        radii_s{i} = diameters/2;
        centers_s{i} = stats.Centroid;

        %-- Clean out any false detected circular objects that are related
        %   to remaining noise if there is any
        if numel(radii_s{i} > 1)
            centers_s{i}(find(radii_s{i}<15),:) = [];
            radii_s{i} = radii_s{i}(radii_s{i}>15);
        end;

    else    %-- If there is no bubble in ROI put empty matrix to cell array
        centers_s{i} = [];
        radii_s{i} = [];
    end;


    %-- If plotting switch vis equals to 1, this part plots detected
    %   circular objects on current frame
    if vis == 1 && isempty(centers_s{i}) == 0
        imshowpair(current_frame{i},dif{i},'montage')
        viscircles(centers_s{i},radii_s{i});
        impixelinfo;
        pause
    end;

    i = i+1;

end
```